Electronic structure of the semimetals Bi and Sb

Yi Liu and Roland E. Allen
Department of Physics, Texas A&M University, College Station, Texas 77843-4242
(Received 22 December 1994; revised manuscript received 13 March 1995)

We have developed a third-neighbor tight-binding model, with spin-orbit coupling included, to treat the electronic properties of Bi and Sb. This model successfully reproduces the features near the Fermi surface that will be most important in semimetal-semiconductor device structures, including (a) the small overlap of valence and conduction bands, (b) the electron and hole effective masses, and (c) the shapes of the electron and hole Fermi surfaces. The present tight-binding model treats these semimetallic properties quantitatively, and it should, therefore, be useful for calculations of the electronic properties of proposed semimetal-semiconductor systems, including superlattices and resonant-tunneling devices.

I. INTRODUCTION

Recently, several groups have reported the successful fabrication of semimetal-semiconductor superlattices, including PbTe-Bi,[1] CdTe-Bi,[2] and GaSb-Sb.[3] Bulk Bi and Sb are group-V semimetals. They have a weak overlap between the valence and conduction bands, which leads to a small number of free electrons and holes. They also exhibit small energy gaps in the vicinity of the Fermi energy. Connected with these properties are high carrier mobilities, small effective masses, and a large characteristic length, which makes Sb and Bi ideal for studying and employing quantum confinement effects. The three above semimetal-semiconductor superlattices are all grown in the [111] direction, along which the electron effective masses of Bi and Sb are relatively small and the quantum confinement length (scaling as m^{*-1}) consequently large. Also, there is only a small lattice mismatch in each case between the (111) planes of semimetal and semiconductor.[1-3] These three systems are, therefore, particularly promising for quantum transport studies and quantum devices.

The semimetals Bi and Sb have an indirect negative band gap, since the conduction-band minima (at the L points) lie (40 meV for Bi, 180 meV for Sb) lower than the valence-band maxima (at the T point for Bi, and H points for Sb).[4] With decreasing thickness of confinement in Bi and Sb, a semimetal-to-semiconductor (SMSC) transition should occur when the energy shift becomes great enough to raise the lowest electron subband to an energy higher than that of the uppermost hole subband. Hoffman *et al.*[5] reported a SMSC transition in CdTe-Bi at a critical Bi-layer thickness of the order of 300 Å.

These indirect narrow-gap semimetal-semiconductor superlattices and heterostructures have been suggested for many potential applications,[6-8] because of their unique transport and optical properties. Resonant tunneling and negative differential resistance have been experimentally observed.[9]

There have been relatively few theoretical attempts to study the electronic and optical properties of these heterostructures. Any model of the band structure faces stringent requirements: (i) The weak overlap and small energy gaps in the vicinity of the Fermi energy for Bi and Sb make a multiband treatment necessary; (ii) the band alignment of these semimetal-semiconductor superlattices is indirect in momentum space, so a theoretical treatment must represent a mixture of bulk states from different symmetry points of the Brillouin zone;[10,11] (iii) the carrier effective masses (particularly along the [111] growth direction) will play an important role in transport properties (including resonant tunneling and the SMSC transition), so a theoretical calculation must treat the effective masses correctly.

The envelope-function approximation uses the effective masses, band gaps, and momentum matrix elements as inputs. It can, therefore, satisfy requirement (iii), and is useful for a superlattice state whose energy is close to a band edge of one of the bulk materials, when only one or two bulk states in each material are of dominant importance.[10] However, this method fails to satisfy requirement (i), because the boundary conditions are extremely complicated when many bands are involved.[11] It is also unsatisfactory with respect to requirement (ii), since it cannot handle a superlattice state derived from two or more bulk states with widely separated wave vectors.[10,11]

The empirical tight-binding (TB) method provides a better theoretical framework for this problem. It takes the effect of the full band structure into account, and the boundary conditions for connecting wave functions across the interface are straightforward. Also, the qualitative behavior of the TB bands near and below the Fermi level is usually in good agreement with experiment. Requirement (iii) above can be approximately satisfied by carefully adjusting the TB parameters to obtain the correct effective masses of the bulk materials. There is a tradeoff, of course: Some properties of the bands are treated less accurately when one focuses on the effective masses, but these are expected to be less important in the superlattice calculations.

Tight-binding models have been widely used for semiconductors.[12,13] There has been much less work on the semimetals Bi and Sb, except for an early effort by Mase[14] and more recent work by Xu *et al.*[15] Mase[14] correctly determined the locations and symmetries of the free carriers of Bi. However, his treatment was not sufficient to

produce a reasonable band structure. Xu *et al.*[15] did more extensive work on As, Sb, and Bi. They fitted their band calculations to first-principles results,[16] and correctly reproduced the overlap and overall band structures. No special attention was paid to the behavior of the bands near the Fermi energy. Their TB model, consequently, does not yield the correct carrier effective masses (and small energy gaps), which are important for further calculations of superlattice states. In this paper, we present an improved model for Bi and Sb. Instead of just considering the overall band structure, we fitted the bands to the detailed experimental data in the vicinity of the Fermi energy, including band overlaps, effective masses of electrons and holes, shape of the Fermi surface at the electron and hole pockets, and small energy gaps. The present model (defined by the parameters of Table II) is thus suitable for studies of superlattices, quantum wells, resonant-tunneling devices, and other semimetal-semiconductor heterostructures.

II. BULK CRYSTAL STRUCTURE

Bulk Bi and Sb have the rhombohedral A7 structure shown in Fig. 1, which is composed of two interpenetrating, trigonally distorted face-centered-cubic lattices with two atoms per unit cell. We take the binary, bisectrix, and trigonal axes to be the x, y, and z directions, respectively. Then the three primitive translation vectors of the lattice are

$$\mathbf{a}_1=(-1/2a,-\sqrt{3}/6a,1/3c)\ , \tag{1}$$

$$\mathbf{a}_2=(1/2a,-\sqrt{3}/6a,1/3c)\ , \tag{2}$$

$$\mathbf{a}_3=(0,\sqrt{3}/3a,1/3c)\ . \tag{3}$$

The three corresponding reciprocal-lattice vectors, defined by

$$\mathbf{b}_i\cdot\mathbf{a}_j=2\pi\delta_{ij}\ , \tag{4}$$

are given by

$$\mathbf{b}_1=(-1,-\sqrt{3}/3,b)g\ , \tag{5}$$

$$\mathbf{b}_2=(1,-\sqrt{3}/3,b)g\ , \tag{6}$$

$$\mathbf{b}_3=(0,2\sqrt{3}/3,b)g\ , \tag{7}$$

where

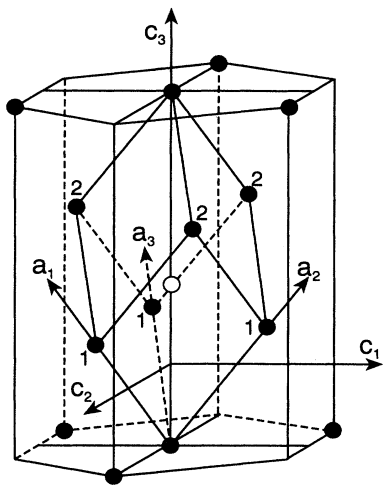

FIG. 1. Crystal structure of Sb and Bi, showing first and second neighbors (labeled 1 and 2) to the central atom represented by an open circle. The bisectrix ($\mathbf{C}_1$), binary ($\mathbf{C}_2$) and trigonal ($\mathbf{C}_3$) axes, and primitive translation vectors ($\mathbf{a}_1$, $\mathbf{a}_2$, $\mathbf{a}_3$) are also shown.

$$b=a/c\ . \tag{8}$$

The relative position of the two basis atoms is given by

$$\mathbf{d}=(0,0,2\mu)c\ . \tag{9}$$

The values of a, c, μ, and g are listed in Table I,[17,18] along with the other lattice parameters for Bi and Sb. The first Brillouin zone for Bi and Sb is shown in Fig. 1.

The A7 structure can be regarded as a distorted cubic structure. It has three nearest neighbors and three second-nearest neighbors. The vectors from a central atom to the nearest neighbors are $\mathbf{a}_1-\mathbf{d}$, $\mathbf{a}_2-\mathbf{d}$, and $\mathbf{a}_3-\mathbf{d}$; those to the second neighbors are $\mathbf{a}_1+\mathbf{a}_2-\mathbf{d}$, $\mathbf{a}_1+\mathbf{a}_3-\mathbf{d}$, and $\mathbf{a}_2+\mathbf{a}_3-\mathbf{d}$.

III. TIGHT-BINDING MODEL

The tight-binding model we use is of the Slater-Koster type.[19] For the group-V elements, the external electron configuration is s^2p^3, plus a complete d shell. Only the s

TABLE I. Crystal structure parameters of Bi and Sb (Refs. 17 and 18) at 4.2 K.

		Bi	Sb
Lattice constants in hexagonal system	a (Å)	4.5332	4.3007
	c (Å)	11.7967	11.2221
Rhombohedral angle	α	57°19′	57°14′
Internal displacement parameter	μ	0.2341	0.2336
Reciprocal-lattice constant	g (Å^{-1})	1.3861	1.4610
Nearest-neighbor distance	d_1 (Å)	3.0624	2.9024
Next-nearest-neighbor distance	d_2 (Å)	3.5120	3.3427

and p states strongly mix to produce the valence and conduction bands of the solid. The basis functions are taken to be orthogonal s and p Löwdin orbitals.[20] The crystal structure of Bi and Sb is rhombohedral, with three nearest, three second-nearest, and six third-nearest neighbors. The relative positions and distances of these neighboring are shown in Fig. 2 and Table I. The first and second neighbors are, respectively, above and below the plane of the central atom.

A reasonable TB model must include second-neighbor interactions for two reasons: (i) Only the combination of nearest- and second-nearest neighbors is sufficient to satisfy all the symmetry requirements of the rhombohedral structure [with the bonding between (111) bilayers eliminated if there are no second-neighbor interactions]; (ii) the values of the distances d_1 and d_2 are very close, so second-neighbor interactions are expected to be significant. Our experience in fitting the bands demonstrates that they do indeed play an important role.

The peculiarity of the band structures of these semimetallic materials is the overlap between the highest valence band and the lowest conduction band, which creates small and equal numbers of free electrons at point L and free holes at point T (for Bi) or point H (for Sb).[4] The question of producing this indirect negative band gap is a delicate one for a tight-binding model. For sp^3-bonded materials with the diamond and zinc-blende structures, Vogl, Hjalmarson, and Dow[12] added an excited s state to the sp^3 basis set for each atom and successfully reproduced the lowest conduction bands even in indirect-gap semiconductors. This s^* state repels the lower antibonding p-like conduction band and presses the indirect conduction-band minima down in energy. The difficulties in extending a TB model to distant neighbors with many adjustable parameters were avoided by introducing an s^* state instead. However, we have found in our calculations that the interaction between the s^* and p states is not adequately selective in the A7 structure. The sp^3s^* model fails to give the fine details of the band structure near the Fermi surface in Bi and Sb.

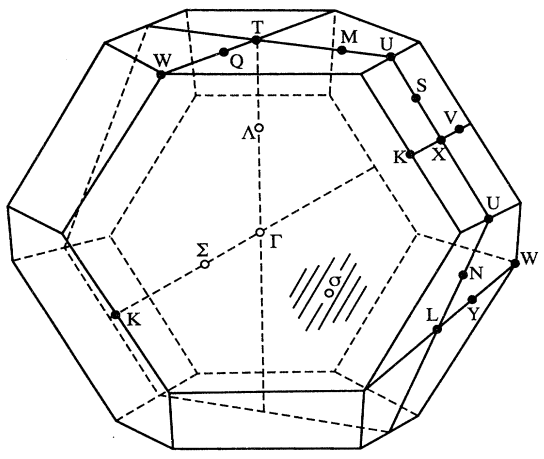

FIG. 2. Brillouin zone for the rhombohedral structure.

Instead of adding an s^* state, we developed an sp^3 model, which includes third-neighbor interactions, but which treats details near the Fermi surface more carefully than the model of Ref. 15. The semimetallicity of Bi and Sb makes it reasonable that the interaction between Löwdin orbitals (or Wannier functions) should extend further than in more covalent systems (with band gaps), like group-IV and III-V semiconductors.

The total Hamiltonian of Bi or Sb is[13]

$$H = H_0 + H_{so} , \tag{10}$$

$$H_{so} = (\hbar/4m^2c^2)[\nabla V \times \mathbf{P}]\cdot\sigma . \tag{11}$$

H_0 is the Hamiltonian without spin-orbit coupling, and H_{so} the spin-orbit component, which couples p orbitals on the same atom. V is the total crystal potential, and σ represents the Pauli spin matrices.

We denote the s and p orbitals on the two atoms of the primitive cell by $|si\sigma\rangle$, $|xi\sigma\rangle$, $|yi\sigma\rangle$, $|zi\sigma\rangle$. The site index i is either 1 or 2, and the spin index σ either $\uparrow$ or $\downarrow$. In this basis, the matrix elements of H_0 with the same spin can be easily calculated by use of the two-center approximation given by Slater and Koster.[19] The spin-orbit component H_{so} can be easily represented in the total angular momentum basis: for example,[13]

$$\langle xi\uparrow|H_{so}|zi\downarrow\rangle = \tfrac{1}{3}\lambda , \tag{12}$$

where λ is the spin-orbit coupling parameter. The transformation[21] between these two bases allows the total Hamiltonian to be expressed in either basis. In the Appendix, we give the expression for the Hamiltonian matrix elements in the $|si\sigma\rangle$, $|xi\sigma\rangle$, $|yi\sigma\rangle$, $|zi\sigma\rangle$ basis.

Our TB model has 14 adjustable parameters: E_s, E_p, $V_{ss\sigma}$, $V_{sp\sigma}$, $V_{pp\sigma}$, $V_{pp\pi}$, $V'_{ss\sigma}$, $V'_{sp\sigma}$, $V'_{pp\sigma}$, $V'_{pp\pi}$, $V''_{ss\sigma}$, $V''_{sp\sigma}$, $V''_{pp\sigma}$, $V''_{pp\pi}$. E_s and E_p are the on-site orbital energies. The unprimed, primed, and double-primed parameters are, respectively, for first, second, and third neighbors. The spin-orbit coupling parameter λ is taken to be approximately 0.6 eV for Sb and 1.5 eV for Bi.[16,22,23]

IV. DETERMINATION OF THE TB PARAMETERS

For the purpose of studying electronic transport and SMSC transitions in semimetal-semiconductor superlattices and heterostructures, we concentrate on features in the energy bands near the Fermi surface instead of the global band structures. We first set out to reproduce (i) the overlap between the highest valence and lowest conduction bands, and (ii) the Fermi energy of the free carriers. These are the basic properties which determine the semimetallicity of Bi and Sb. In our calculations, however, we found that the overlap and Fermi energy are insensitive to the TB parameters, and can be obtained correctly from different sets of parameters. Another important consideration is (iii) the effective masses of the free carriers, especially along the [111] direction. This is the growth direction for the semimetal-semiconductor superlattices in which we are interested. The effective mass is important for determining the SMSC transition and the transport properties, and must, therefore, be fitted carefully. Still another important factor is (iv) the shape of

the Fermi surfaces for electrons and holes. The external momenta and external areas are very sensitive to the TB parameters. The density of free carriers (n or p with $n=p$) is determined by the volume of the electron and hole pockets. The final important feature is (v) the band gaps near the Fermi level. In Bi, the L point, where the electron pocket is located, has a direct energy gap of 13.6 meV (Ref. 24) at low temperature. Nonparabolicity is expected to be important in this case. We also were concerned with the band structure farther away from the Fermi level, but this is the least important aspect for our purposes, and was taken into account only when there was no risk of inordinately compromising the first five properties.

Several semiconductors with the diamond or zinc-blende structure contain Sb or elements near to Sb and Bi in the periodic table. These include α-Sn, InSb, and GaSb, for which TB parameters have been determined by several authors.[12,13] To obtain the first and second-neighbor-interaction parameters for Sb and Bi, we assume that the parameters of α-Sn, InSb, and GaSb and those of Sb and Bi are connected by a d^{-2} scaling rule.[25] (The crystal symmetries are different, of course: α-Sn, InSb, and GaSb are cubic, while Bi and Sb are rhombohedral.) The parameters obtained from this scaling are then adjusted slightly to fit the theoretical curves to the existing experimental data, with emphasis on properties (i)–(v) discussed above. The third-neighbor interactions are regarded as small perturbations, adjusted freely without imposing the d^{-2} rule (see Fig. 3).

For materials having the diamond or zinc-blende structure, with only nearest-neighbor interactions included, it is a simple matter to relate the TB parameters to the energy bands at high-symmetry points in the Brillouin zone.[12,13,25] In this case, the TB parameters can be easily adjusted to fit the experimental data. In our fits, however, we have to deal with (a) the lower-symmetry rhombohedral structure, (b) third-neighbor interactions, and (c) the spin-orbit coupling. The Hamiltonian matrices of Bi and Sb are consequently much more complicated even at high-symmetry points of the BZ.

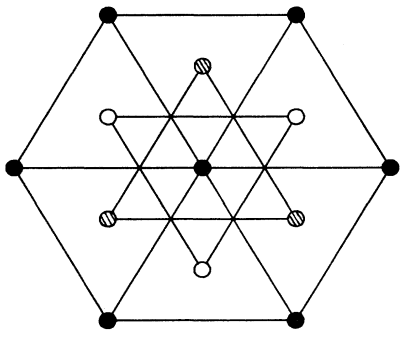

FIG. 3. Positions of the first-, second-, and third-nearest neighbors projected onto the plane perpendicular to the trigonal axis. The three first- and three second-nearest neighbors are in the planes above and below the plane in which the central atom lies, while the six third-nearest neighbors are in the same plane as the central atom. (●—central atom and third neighbors; ○—nearest neighbors; ⦻—second neighbors.)

Within the TB model described previously, the explicit expressions for two of the bands along the Γ-T ([111]) direction are given by

$$E(\Gamma_{45}^{\mp}-T_{45}^{\pm})=E_p+3(V''_{pp\sigma}+V''_{pp\pi})+1/3\lambda \pm\sqrt{m^2+l^2+2ml\cos(\mathbf{a}_1\cdot\mathbf{k})}\ , \tag{13}$$

where $\mathbf{k}=(u,u,u)$ with $0\le u\le 0.5$, and

$$m=2\cos^2\alpha V_{pp\sigma}+(3-2\cos^2\alpha)V_{pp\pi}\ , \tag{14}$$

$$l=2\cos^2\alpha' V'_{pp\sigma}+(3-2\cos^2\alpha')V'_{pp\pi}\ . \tag{15}$$

For the Γ Point, $\mathbf{k}=(0,0,0)$, Eq. (13) gives

$$E(\Gamma_{45}^{\mp})=E_p+3(V''_{pp\sigma}+V''_{pp\pi})+1/3\lambda\pm|m+l|\ . \tag{16}$$

For the T Point, $\mathbf{k}=(0.5,0.5,0.5)$, Eq. (13) gives

$$E(T_{45}^{\pm})=E_p+3(V''_{pp\sigma}+V''_{pp\pi})+1/3\lambda\pm|m-l|\ . \tag{17}$$

The bandwidth associated with (16) and (17)

$$\Delta(T_{45}^{\pm}-\Gamma_{45}^{\mp})=4\cos^2\alpha' V'_{pp\sigma}+(6-4\cos^2\alpha')V'_{pp\pi}\ . \tag{18}$$

Note that $\Delta(T_{45}^{\pm}-\Gamma_{45}^{\mp})$ is only determined by the second-neighbor interaction parameters $V'_{pp\sigma}$ and $V'_{pp\pi}$.

In Bi, the hole pocket is at the T point with symmetry T_{45}^{-}.[14,18] From Eq. (13), we can derive an explicit expression for the effective mass of the hole at the maximum of the band along the [111] direction:

$$m_h^{*-1}=\frac{c^2}{9\hbar^2}\frac{ml}{|m-l|}\ . \tag{19}$$

Equation (19) is quite useful when we fit the effective masses of the free carriers.

We find, to an excellent approximation, that $V_{ss\sigma}$ and $V'_{ss\sigma}$ can be related to the energies of the two lowest-lying valence bands at the Γ and T points. At Γ, the relations are

$$E(\Gamma_6^{\pm})=E_s+6V''_{ss\sigma}\pm A+B^2/[E_s+6V''_{ss\sigma}-E_p -6V''_{pp\pi}\pm(A+C)]\ , \tag{20}$$

where

$$A=3(V_{ss\sigma}+V'_{ss\sigma})\ , \tag{21}$$

$$B=3(V_{sp\sigma}\cos\gamma+V'_{sp\sigma}\cos\gamma')\ , \tag{22}$$

$$C=3(V_{pp\sigma}\cos^2\gamma+V_{pp\pi}\sin^2\gamma) +3(V'_{pp\sigma}\cos^2\gamma'+V'_{pp\pi}\sin^2\gamma')\ . \tag{23}$$

If $|A+C|$, $|B|\ll|E_s-E_p|$ is well satisfied, we can obtain a simple expression for the energy difference of the Γ_6^+ and Γ_6^- states:

$$E(\Gamma_6^-)-E(\Gamma_6^+)=|6(V_{ss\sigma}+V'_{ss\sigma})|\ . \tag{24}$$

At T, the relations are

$$E(T_6^{\pm})=E_s+6V''_{ss\sigma}\pm A'+B'^2/[E_s+6V''_{ss\sigma}-E_p -6V''_{pp\pi}\pm(A'+C')]\ , \tag{25}$$

TABLE II. Nearest-neighbor distance d_1 and second-nearest-neighbor distance d_2 (in Å) and TB parameters for Bi, Sb, α-Sn, InSb, and GaSb. Those of α-Sn, InSb, and GaSb are obtained from Ref. 12. For the compounds, the upper value of E_s or E_p corresponds to the anion, and the lower to the cation. The upper (lower) $V_{sp\sigma}$ corresponds to the s orbital on the anion (cation), and a p orbital on its nearest neighbor.

	d_1	d_2	E_s	E_p	$V_{ss\sigma}$	$V_{sp\sigma}$	$V_{pp\sigma}$	$V_{pp\pi}$
Bi	3.062	3.512	−10.906	−0.486	−0.608	1.320	1.854	−0.600
Sb	2.902	3.343	−10.068	−0.926	−0.694	1.554	2.342	−0.582
α-Sn	2.81		−5.670	1.330	−1.417	1.953	2.373	−0.687
InSb	2.81		−8.016	0.674	−1.380	1.640	2.289	−0.619
			−3.464	2.916		1.987		
GaSb	2.64		−7.321	0.855	−1.539	2.148	2.459	−0.637
			−3.899	2.915		2.021		
	$V'_{ss\sigma}$	$V'_{sp\sigma}$	$V'_{pp\sigma}$	$V'_{pp\pi}$	$V''_{ss\sigma}$	$V''_{sp\sigma}$	$V''_{pp\sigma}$	$V''_{pp\pi}$
Bi	−0.384	0.433	1.396	−0.344	0	0	0.156	0
Sb	−0.366	0.478	1.418	−0.393	0	0	0.352	0

where

$$A' = -3(V_{ss\sigma} - V'_{ss\sigma}) , \tag{26}$$

$$B' = -3(V_{sp\sigma}\cos\gamma - V'_{sp\sigma}\cos\gamma') , \tag{27}$$

$$C' = -3(V_{pp\sigma}\cos^2\gamma + V_{pp\pi}\sin^2\gamma) + 3(V'_{pp\sigma}\cos^2\gamma' + V'_{pp\pi}\sin^2\gamma') . \tag{28}$$

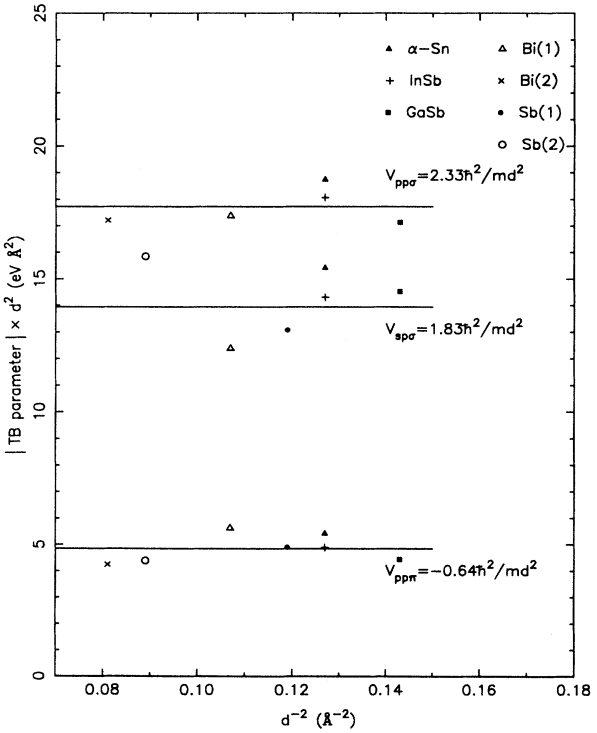

FIG. 4. Interatomic TB parameters $V_{pp\sigma}(V'_{pp\sigma})$, $V_{pp\pi}(V'_{pp\pi})$, and $V_{sp\sigma}$ multiplied by the square of the bond length, vs the bond length d. $V_{sp\sigma}$ for the compounds InSb and GaSb is obtained by averaging the two values in Table II.

If $|A'+C'|$, $|B'| \ll |E_s - E_p|$ is well satisfied, it follows that

$$E(T_6^+) - E(T_6^-) = |6(V_{ss\sigma} - V'_{ss\sigma})| . \tag{29}$$

For Bi and Sb, since the s levels lie about 9 eV lower than the p levels,[16] the above two inequalities are usually true.

Equations (24) and (29) are used to fit the two lowest valence bands, while Eqs. (13), (16), and (17) are used for the higher-lying valence and conduction bands. Equation (19) gives the exact formula for the effective mass of the hole at the maximum of the valence band along the [111] direction.

The TB parameters, which give the best agreement with experimental data, are presented in Table II, along with the parameters for α-Sn, InSb, and GaSb. The values of $V_{ss\sigma}$ and $V'_{ss\sigma}$ of Bi and Sb obtained from these three cubic semiconductors by assuming d^{-2} scaling fail to produce the experimental results for the two lowest-lying valence bands. The values in Table II are calculated from Eqs. (24) and (29), instead of the d^{-2} scaling rule. However, when the values of $V_{sp\sigma}$, $V_{pp\sigma}$, $V'_{pp\sigma}$, and $V'_{pp\pi}$ are plotted against the bond length in Fig. 4, d^{-2} scaling is found to be approximately satisfied. We mention that

TABLE III. Energy levels of Bi (in eV) at the symmetry points T, Γ, L, and X.

T_6^-	−12.2442	Γ_6^+	−14.0000	L_s	−11.9545	X_a	−12.1649
T_6^+	−11.1331	Γ_6^-	−8.0870	L_a	−11.5966	X_s	−10.3162
T_6^-	−1.1798	Γ_6^+	−2.5364	L_s	−1.7896	X_s	−5.6525
T_6^+	−1.1196	Γ_6^+	−1.1289	L_a	−1.6669	X_a	−4.1632
T_{45}^-	0.0111	Γ_{45}^+	−0.8238	L_a	−0.0403	X_a	−3.1047
T_6^+	0.3813	Γ_6^-	0.2430	L_s	−0.0267	X_s	2.3508
T_6^-	0.9529	Γ_6^-	1.6893	L_s	0.8024	X_s	3.2956
T_{45}^+	1.4754	Γ_{45}^-	1.7878	L_a	0.9201	X_a	4.4031

TABLE IV. Comparison of characteristic energy levels (in eV) for Bi with other calculations and with experimental data.

Band	Present calculation	Golin (Ref. 18)	Xu (Ref. 15)	Experiment[a] Value	Ref.
$\Gamma_6^+(1)$	−14.00	−10.50	−13.32	−14.0	29
$\Gamma_6^-(1)$	−8.09	−6.55	−7.53	−8.1	29
$T_6^+(1)$-$T_6^-(1)$	1.11	1.78	2.39	1.18±0.08	29
$L_a(1)$-$L_s(1)$	0.36	0.58	0.74		
$X_s(2)$	−5.65	−3.70		−5.2	29
$\Gamma_6^-(2)$-$\Gamma_{45}^+(1)$	1.07	0.83	1.61	0.65–0.71	30,31
$\Gamma_6^-(2)$-$\Gamma_6^+(3)$	1.37	0.82	1.97	0.72–0.81	30,31
$T_6^+(3)$-$T_{45}^-(1)$	0.370	0.505	0.756	0.18–0.41	32–36
$T_6^-(3)$-$T_{45}^-(1)$	0.94	0.87	0.99	0.80–0.88	31
$T_6^+(2)$-$T_{45}^-(1)$	−1.13	−1.60	−1.23		
$L_a(3)$-$L_s(3)$	−0.014	−0.015	−0.874	−0.011–−0.015	24,33,37–39
$L_a(2)$-$L_s(3)$	−1.64	−1.82	−2.24	−1.92–−2.10	30,31
$L_s(4)$-$L_a(3)$	0.84	1.13	1.73	1.05–1.15	30,31
$L_s(4)$-$L_s(3)$	0.83	1.12	0.86		
$T_{45}^-(1)$-$L_s(3)$	0.038	0.039	0.040	0.036–0.039	32,33,39,40

[a]See the references for experimental conditions.

the difference in E_s and E_p for Sb atoms in bulk Sb, GaSb, and InSb can be interpreted as arising from the different local environments in these three materials.[26,27]

V. BAND STRUCTURE OF Bi

The calculated band structure of Bi is shown in Fig. 5, with the zero of energy taken to be Fermi level. The energies at the symmetry points T, Γ, L, and X are given in Table III. The ordering of energy levels is the same as that of Rose and Schuchardt,[28] but different from that of Golin,[18] with the $\Gamma_6^+(3)$ and $\Gamma_{45}^+(1)$ interchanged. Table IV presents a comparison with other theoretical results and with experimental data.

For the two lowest-lying valence bands, our results are in better agreement with experimental data than those from the pseudopotential calculation of Golin.[18] (Xu *et al.*[15] fitted their model to the calculation of Gonze, Michenaud, and Vigneron[16] instead of the experimental data.) This demonstrates that a TB model can provide a good representation of the lower-lying valence bands.

It can be seen that the Fermi level intersects the valence band at the T point, and the conduction band at L. The overlap between them, $E[T_{45}^-(1)-L_s(3)]$, is 38 meV. There are many band energies near the Fermi level. The smallest band gap, at the L point, is only about 14 meV. This is $E[L_a(3)-L_s(3)]$. The band gap at T is about 370 meV $\{E[T_6^+(3)-T_{45}^-(1)]\}$. We can repro-

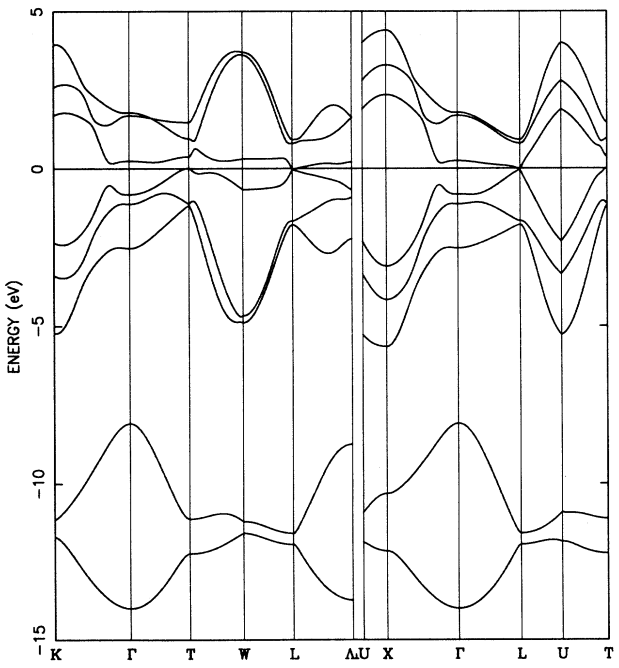

FIG. 5. Band structure of Bi along various symmetry lines. The notation used here is the same as that of Golin (Ref. 18).

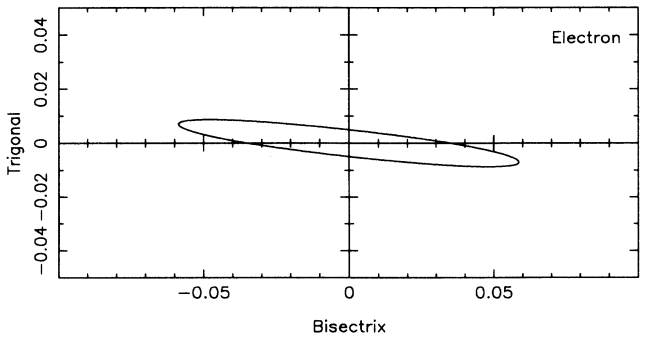

FIG. 6. Fermi surface of electrons in the trigonal-bisectrix plane for Bi. The unit of reciprocal length is $g=1.386$ Å^{-1}.

TABLE V. Theoretical and experimental parameters for Fermi surface and effective masses[a] of Bi. The notation for direction is that used by Edel'man (Ref. 41).

	Present work	Rose and Schuchardt (Ref. 28)	Experiment[b] Values	Ref.
Overlap E_0 (meV)	37.8	24.0	36.0–38.5	32,33,39,40
Fermi energy E_f^e (meV)	26.7	16.0	25.0–29.7	32,33,39,40,42
		Electrons		
Tilt angle θ	6.0°	8.2°	6°23′±1′	41
P_1 (10^{-21} g cm/s)	8.615	6.60	7.88±0.2 %	
P_2	0.589	0.599	0.559±0.2 %	41
P_3	0.714	0.675	0.740±0.2 %	
m_1^c (m_e)	0.198	0.235[d]	0.261	
m_2^c	0.001 47	0.001 94[d]	0.001 13	40
m_3^c	0.002 15	0.002 46[d]	0.002 59	
		Holes		
Tilt angle θ	0°	0°	0°	41
P_1 (10^{-21} g cm/s)	1.543	1.56	1.47	
P_2	1.534	1.56	1.47	41
P_3	4.547	5.89	4.88	
m_1 (m_e)	0.0675	0.097[d]	0.064	
m_2	0.0675	0.096[d]	0.064	33,40,41,43
m_3	0.612	1.37[d]	0.690–0.702	
		Carrier density (cm^{-3})		
n^e	3.09×10^{17}			
p^e	3.12×10^{17}		$(2.75–3.02)\times10^{17}$	33,40,41,43
n/p	0.99		1	

[a]Effective masses for the principal axes.
[b]See the references for experimental conditions.
[c]Effective masses at the bottom of the band.
[d]Obtained from Lax model. See Ref. 28.
[e]Obtained by assuming that the electron and hole pockets are ellipsoids.

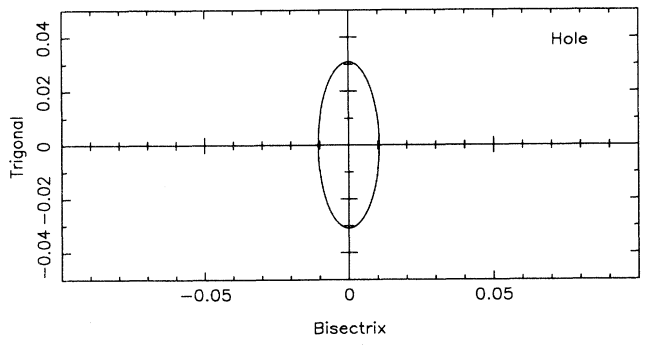

FIG. 7. Fermi surface of holes in the trigonal-bisectrix plane for Bi. The unit of reciprocal length is $g = 1.386$ Å^{-1}.

duce these three characteristic energy values in good agreement with both the experimental data and the pseudopotential calculations,[18] and as shown in Table IV.

The small direct band gap at L, which is only about

TABLE VI. Energy levels of Sb (in eV) at the symmetry points T, Γ, L, and X.

T_6^-	−12.022	Γ_6^+	−13.446	L_s	−11.659	X_a	−11.607
T_6^+	−10.378	Γ_6^-	−7.150	L_a	−11.156	X_s	−9.916
T_6^-	−1.252	Γ_6^+	−2.684	L_s	−2.421	X_s	−6.571
T_{45}^-	−0.814	Γ_6^+	−1.759	L_a	−2.145	X_a	−4.730
T_6^+	−0.332	Γ_{45}^+	−1.454	L_s	−0.786	X_a	−4.217
T_6^+	0.732	Γ_6^-	1.076	L_a	−0.0899	X_s	2.579
T_6^-	1.125	Γ_6^-	1.836	L_s	0.166	X_s	3.229
T_{45}^+	1.474	Γ_{45}^-	2.114	L_a	0.991	X_a	4.135

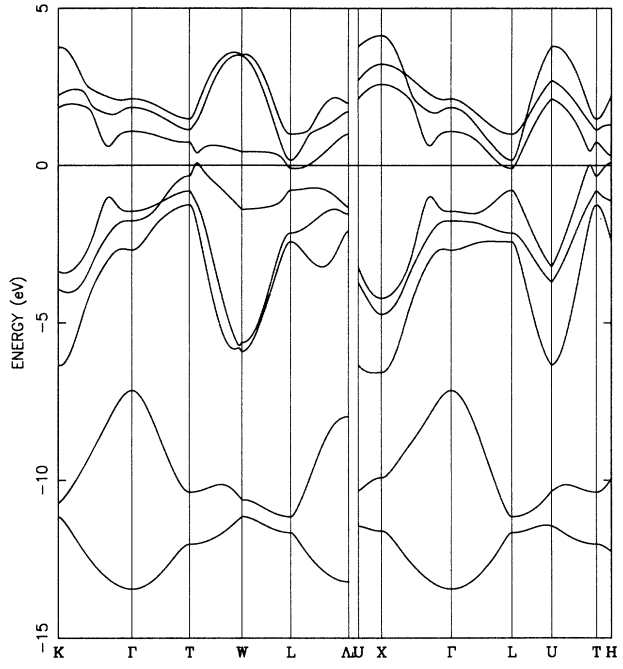

FIG. 8. Band structure of Sb along various symmetry lines. The notation used here is the same as that of Falicov and Lin (Ref. 17).

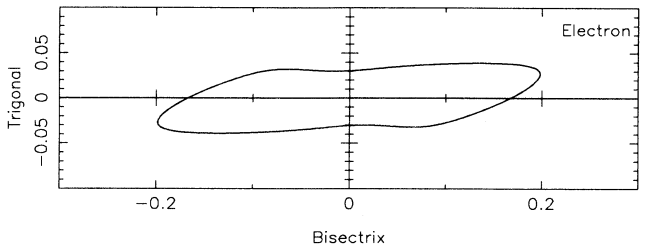

FIG. 9. Fermi surface of electrons in the trigonal-bisectrix plane for Sb. The unit of reciprocal length is $g = 1.461$ Å^{-1}.

one-third of the overlap energy, has an important influence on the transport properties of Bi. The strong coupling between the conduction and valence bands, and the resulting nonparabolic band dispersion, should be taken into account when calculating superlattice states. Also note that the small effective masses are usually associated with small energy gaps. For bismuth, the electron effective mass along the trigonal axis at the L point is smaller than $3\times10^{-3}m_e$, which means that large quantum confinement is expected for Bi (Sec. I). In fact, our calculated effective masses are in very good agreement with the experimental data. The comparison of our results with other theoretical and experimental values for the Fermi surface and carrier effective masses is summarized in Table V. Figures 6 and 7 show the calculated electron and hole pockets. It is clear that there is excellent agreement.

The previous TB calculation of Xu *et al.*[15] gave a large value for the band gap at L (874 meV). The related electron effective masses are expected to be far away from the experimental data. This casts doubt on the reliability of their model for treating transport and other properties in semimetal-semiconductor quantum structures.

VI. BAND STRUCTURE OF Sb

The calculated band structure of Sb is shown in Fig. 8. The zero of energy is taken to be the Fermi level. The energies at the symmetry points T, Γ, L, and X are listed in Table VI. The ordering of energy levels is essentially the same as that of Rose and Schuchardt;[28] only $T_6^-(3)$ and $T_{45}^+(1)$ are interchanged. A comparison with other theoretical results and with experimental data is presented in Table VII.

As in the case of Bi, our results for the two lowest-lying valence bands are in better agreement with experimental data than those of a pseudopotential calculation—for Sb, that of Falicov and Lin.[17]

In our calculation, the maximum of the fifth band

TABLE VII. Comparison of characteristic energy levels (in eV) for Sb with other calculations and with experimental data.

Band	Present calculation	Falicov and Lin (Ref. 17)	Xu *et al.* (Ref. 15)	Experiment[a] Values	Ref.
$\Gamma_6^+(1)$	−13.45	−12.10	−12.87	−13.3	29
$\Gamma_6^-(1)$	−7.15	−6.15	−5.17	−7.0	29
$T_6^+(1)$-$T_6^-(1)$	1.64	1.71	2.9	1.67±0.06	29
$L_a(1)$-$L_s(1)$	0.50	0.54	0.94		
$X_s(1)$-$X_a(1)$	1.69	1.90			
$X_s(2)$	−6.57	−4.79		−5.5	29
$T_6^+(2)$-$T_{45}^-(1)$	0.48	0.63	0.64	0.143	44
$T_6^+(3)$-$T_6^+(2)$	1.06	0.98	1.32		
$L_s(3)$-$L_a(3)$	−0.70	−0.24	−0.34	−0.101±0.003	44–46
$L_a(2)$-$L_s(3)$	−1.36	−1.11	−1.31		

[a]See the references for experimental conditions.

TABLE VIII. Theoretical and experimental parameters of Fermi surface and effective masses of Sb. The notation for directions is that used by Issi (Ref. 4).

	Present work	Rose and Schuchardt (Ref. 28)	Experiment[a] Values	Ref.
Overlap E_0 (meV)	17.40	234	177.5	4
Fermi energy E_f^e (meV)	89.9	115	93.1	4
		Electrons		
Tilt angle $\theta_{\max}$	$-8.5°$	$-6°$	$-4°--7°$	47–49
P_1 (10^{-21} g cm/s)	4.30	5.2	3.95	
P_2	30.82	32.3	31.30	49
P_3	4.62	3.6	4.22	
$m_{[111]}$ (m_e)	0.073		0.093[b]	4,47
		Holes		
Tilt angle $\theta_{\min}$	24°	56°	53°	48,49
P_1 (10^{-21} g cm/s)	5.11		4.22	
P_2	19.41	20.2	18.45	49
P_3	3.00	4.4	4.43	
$m_{[111]}$ (m_e)	0.12		0.091[b]	4,47
		Carrier density (cm^{-3})		
n[c]	5.32×10^{19}			
p[c]	5.17×10^{19}		$(3.74-5.50)\times10^{19}$	48,50,51
n/p	1.03		1	

[a]See the references for experimental conditions.
[b]Calculated from the formula $1/m=(\lambda_1^2/m_1)+(\lambda_2^2/m_2)+(\lambda_3^2/m_3)$. Here m_1, m_2, and m_3 are the effective masses along the principal axes, and λ_1, λ_2, and λ_3 are the direction cosines of the trigonal axis in the principal-axis coordinates.
[c]Calculated by assuming the electron and hole pockets are ellipsoids.

occurs at the point H, which is near the point T. (H is on the mirror plane, with trigonal coordinates [0.4543, 0.3722, 0.3722].) The minimum of the sixth band occurs at points near or at L. The overlap of these bands is 174 meV.

The cross sections of the electron pockets and hole pockets on the mirror plane are shown in Figs. 9 and 10, respectively. The Fermi surface results are given in Table VIII, and are compared with other theoretical and experimental data.

For the hole pocket, our calculated tilt angle is 24°, which is the only feature significantly different from experiment data. The shapes of the hole pocket and electron pocket are generally in agreement with those given

TABLE IX. The matrix elements of H_{11}.

	$s1\uparrow$	$s1\downarrow$	$x1\uparrow$	$y1\uparrow$	$z1\uparrow$	$x1\downarrow$	$y1\downarrow$	$z1\downarrow$
$s1\uparrow$	$E_s+g_{26}V''_{ss\sigma}$	0	$g_{27}V''_{sp\sigma}$	$g_{28}V''_{sp\sigma}$	0	0	0	0
$s1\downarrow$		$E_s+g_{26}V''_{ss\sigma}$	0	0	0	$g_{27}V''_{sp\sigma}$	$g_{28}V''_{sp\sigma}$	0
$x1\uparrow$			$E_p+g_{29}V''_{pp\sigma}$ $+g_{30}V''_{pp\pi}$	$-i\frac{1}{3}\lambda$ $+g_{31}(V''_{pp\sigma}-V''_{pp\pi})$	0	0	0	$\frac{1}{3}\lambda$
$y1\uparrow$				$E_p+g_{30}V''_{pp\sigma}$ $+g_{29}V''_{pp\pi}$	0	0	0	$-i\frac{1}{3}\lambda$
$z1\uparrow$					$E_p+g_{26}V''_{pp\pi}$	$-\frac{1}{3}\lambda$	$i\frac{1}{3}\lambda$	0
$x1\downarrow$						$E_p+g_{29}V''_{pp\sigma}$ $+g_{30}V''_{pp\pi}$	$i\frac{1}{3}\lambda+g_{31}(V''_{pp\sigma}-V''_{pp\pi})$	0
$y1\downarrow$							$E_p+g_{30}V''_{pp\sigma}$ $+g_{29}V''_{pp\pi}$	0
$y1\downarrow$								
$z1\downarrow$								$E_p+g_{26}V''_{pp\pi}$

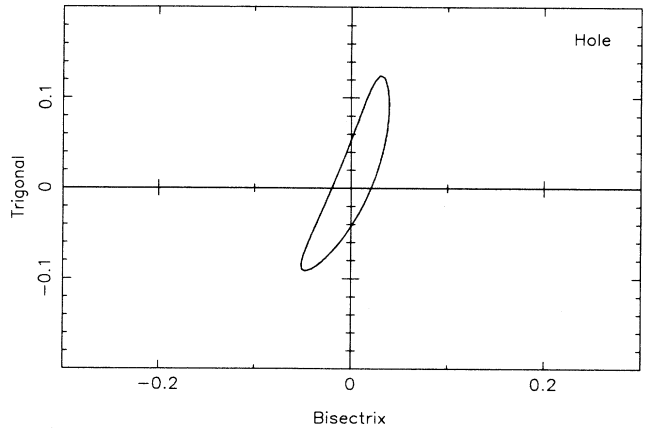

FIG. 10. Fermi surface of holes in the trigonal-bisectrix plane for Sb. The unit of reciprocal length is $g=1.461$ Å^{-1}.

by experiment. Since we cannot quantitatively reproduce the carrier effective masses along all three principal axes, we focus on those along the trigonal axis—i.e., the growth [111] direction for CdTe-Bi, PbTe-Bi, and GaSb-Sb superlattices. Our calculated effective masses along the [111] direction, listed in Table VIII, are in good agreement with the experimental measurements.

VII. CONCLUSIONS

The electronic band structures of bismuth and antimony have been successfully represented with a tight-binding model. The orbital interaction parameters were determined by fitting the experimental data, which include the following: (1) the overlap between the highest valence band and the lowest conduction band; (2) the Fermi energy; (3) the effective masses of the carriers at the minima of the conduction band and at the maxima of the valence band; (4) the shapes of the Fermi surfaces for both electrons and holes; and (5) the small band gaps. Particular attention was given to the behavior of the bands in the vicinity of the Fermi surface, since it is this behavior that will dominantly influence the electronic properties important for device applications.

APPENDIX

This Appendix gives the explicit expressions for the Hamiltonian matrix elements in the representation $|si\sigma\rangle$, $|xi\sigma\rangle$, $|yi\sigma\rangle$, and $|zi\sigma\rangle$. The site index $i=1,2$ distinguishes which represents the two atoms in the primitive cell:

$$H=\begin{bmatrix} H_{11} & H_{12} \\ H_{21} & H_{22} \end{bmatrix}.$$

The diagonal matrix $H_{11}=H_{22}$ and the off-diagonal matrix $H_{12}=H_{21}^{\dagger}$ are presented in Tables IX and X, respectively.

TABLE X. The matrix elements of H_{12}.

	$s2\uparrow$	$s2\downarrow$	$x2\uparrow$	$y2\uparrow$	$z2\uparrow$	$x2\downarrow$	$y2\downarrow$	$z2\downarrow$
$s1\uparrow$	$g_0V_{ss\sigma}+g_{13}V'_{ss\sigma}$	0	$g_1V_{sp\sigma}+g_{14}V'_{sp\sigma}$	$g_2V_{sp\sigma}+g_{15}V'_{sp\sigma}$	$g_3V_{sp\sigma}+g_{16}V'_{sp\sigma}$	0	0	0
$s1\downarrow$	0	$g_0V_{ss\sigma}+g_{13}V'_{ss\sigma}$	0	0	0	$g_1V_{sp\sigma}+g_{14}V'_{sp\sigma}$	$g_2V_{sp\sigma}+g_{15}V'_{sp\sigma}$	$g_3V_{sp\sigma}+g_{16}V'_{sp\sigma}$
$x1\uparrow$	$-g_1V_{sp\sigma}-g_{14}V'_{sp\sigma}$	0	$g_4V_{pp\sigma}+g_5V_{pp\pi}$ $+g_{17}V'_{pp\sigma}+g_{18}V'_{pp\pi}$	$g_{12}(V_{pp\sigma}-V_{pp\pi})$ $+g_{25}(V'_{pp\sigma}-V'_{pp\pi})$	$g_6(V_{pp\sigma}-V_{pp\pi})$ $+g_{19}(V'_{pp\sigma}-V'_{pp\pi})$	0	0	0
$y1\uparrow$	$-g_2V_{sp\sigma}-g_{15}V'_{sp\sigma}$	0	$g_{12}(V_{pp\sigma}-V_{pp\pi})$ $+g_{25}(V'_{pp\sigma}-V'_{pp\pi})$	$g_7V_{pp\sigma}+g_8V_{pp\pi}$ $+g_{20}V'_{pp\sigma}+g_{21}V'_{pp\pi}$	$g_{11}(V_{pp\sigma}-V_{pp\pi})$ $+g_{24}(V'_{pp\sigma}-V'_{pp\pi})$	0	0	0
$z1\uparrow$	$-g_3V_{sp\sigma}-g_{16}V'_{sp\sigma}$	0	$g_6(V_{pp\sigma}-V_{pp\pi})$ $+g_{19}(V'_{pp\sigma}-V'_{pp\pi})$	$g_{11}(V_{pp\sigma}-V_{pp\pi})$ $+g_{24}(V'_{pp\sigma}-V'_{pp\pi})$	$g_9V_{pp\sigma}+g_{10}V_{pp\pi}$ $+g_{22}V'_{pp\sigma}+g_{23}V'_{pp\pi}$	0	0	0
$x1\downarrow$	0	$-g_1V_{sp\sigma}-g_{14}V'_{sp\sigma}$	0	0	0	$g_4V_{pp\sigma}+g_5V_{pp\pi}$ $+g_{17}V'_{pp\sigma}+g_{18}V'_{pp\pi}$	$g_{12}(V_{pp\sigma}-V_{pp\pi})$ $+g_{25}(V'_{pp\sigma}-V'_{pp\pi})$	$g_6(V_{pp\sigma}-V_{pp\pi})$ $+g_{19}(V'_{pp\sigma}-V'_{pp\pi})$
$y1\downarrow$	0	$-g_2V_{sp\sigma}-g_{15}V'_{sp\sigma}$	0	0	0	$g_{12}(V_{pp\sigma}-V_{pp\pi})$ $+g_{25}(V'_{pp\sigma}-V'_{pp\pi})$	$g_7V_{pp\sigma}+g_8V_{pp\pi}$ $+g_{20}V'_{pp\sigma}+g_{21}V'_{pp\pi}$	$g_{11}(V_{pp\sigma}-V_{pp\pi})$ $+g_{24}(V'_{pp\sigma}-V'_{pp\pi})$
$z1\downarrow$	0	$-g_3V_{sp\sigma}-g_{16}V'_{sp\sigma}$	0	0	0	$g_6(V_{pp\sigma}-V_{pp\pi})$ $+g_{19}(V'_{pp\sigma}-V'_{pp\pi})$	$g_{11}(V_{pp\sigma}-V_{pp\pi})$ $+g_{24}(V'_{pp\sigma}-V'_{pp\pi})$	$g_9V_{pp\sigma}+g_{10}V_{pp\pi}$ $+g_{22}V'_{pp\sigma}+g_{23}V'_{pp\pi}$

In these tables, g_0, $g_1, \ldots, g_{31}$ are functions of the reciprocal-lattice vector $\mathbf{k}=k_1\mathbf{b}_1+k_2\mathbf{b}_2+k_3\mathbf{b}_3$, with $\mathbf{b}_1$, $\mathbf{b}_2$, and $\mathbf{b}_3$ the primitive reciprocal-lattice vectors defined in Sec. II. Among them, g_0-g_{12} involve the first-neighbor interactions, g_{13}-g_{25} the second neighbors, and g_{26}-g_{31} the third neighbors. The expressions for g_0-g_{12} are

$$g_0=e^{i\mathbf{k}\cdot(\mathbf{a}_1-\mathbf{d})}+e^{i\mathbf{k}\cdot(\mathbf{a}_2-\mathbf{d})}+e^{i\mathbf{k}\cdot(\mathbf{a}_3-\mathbf{d})} ,$$

$$g_1=(e^{i\mathbf{k}\cdot(\mathbf{a}_2-\mathbf{d})}-e^{i\mathbf{k}\cdot(\mathbf{a}_1-\mathbf{d})})\cos\alpha ,$$

$$g_2=(e^{i\mathbf{k}\cdot(\mathbf{a}_1-\mathbf{d})}+e^{i\mathbf{k}\cdot(\mathbf{a}_2-\mathbf{d})}-2e^{i\mathbf{k}\cdot(\mathbf{a}_3-\mathbf{d})})\cos\beta ,$$

$$g_3=g_0\cos\gamma ,$$

$$g_4=(e^{i\mathbf{k}\cdot(\mathbf{a}_1-\mathbf{d})}+e^{i\mathbf{k}\cdot(\mathbf{a}_2-\mathbf{d})})\cos^2\alpha ,$$

$$g_5=g_0-g_4 ,$$

$$g_6=g_1\cos\gamma ,$$

$$g_7=(e^{i\mathbf{k}\cdot(\mathbf{a}_1-\mathbf{d})}+e^{i\mathbf{k}\cdot(\mathbf{a}_2-\mathbf{d})}+4e^{i\mathbf{k}\cdot(\mathbf{a}_3-\mathbf{d})})\cos^2\beta ,$$

$$g_8=g_0-g_7 ,$$

$$g_9=g_0\cos^2\gamma ,$$

$$g_{10}=g_0\sin^2\gamma ,$$

$$g_{11}=g_2\cos\gamma ,$$

$$g_{12}=g_1\cos\beta ,$$

with $\mathbf{a}_1$, $\mathbf{a}_2$, $\mathbf{a}_3$, and $\mathbf{d}$ defined in Sec. II. Here $\cos\alpha$, $\cos\beta$, and $\cos\gamma$ are the direction cosines for the vector $\mathbf{a}_2-\mathbf{d}$, from the central atom to one of the nearest-neighbor atoms. The functions $g_{13}-g_{25}$ can be obtained by replacing $\mathbf{a}_1$, $\mathbf{a}_2$, $\mathbf{a}_3$, $\cos\alpha$, $\cos\beta$, and $\cos\gamma$ in the expressions for g_0-g_{12} by $\mathbf{a}_2+\mathbf{a}_3$, $\mathbf{a}_1+\mathbf{a}_3$, $\mathbf{a}_2+\mathbf{a}_1$, $\cos\alpha'$, $\cos\beta'$, and $\cos\gamma'$, respectively, where $\cos\alpha'$, $\cos\beta'$, and $\cos\gamma'$ are the direction cosines for the vector $\mathbf{a}_1+\mathbf{a}_3-\mathbf{d}$, from the central atom to one of the second-neighbor atoms. Finally, $g_{26}-g_{31}$ are given by

$$g_{26}=e^{i\mathbf{k}\cdot(\mathbf{a}_1-\mathbf{a}_2)}+e^{i\mathbf{k}\cdot(\mathbf{a}_2-\mathbf{a}_1)}+e^{i\mathbf{k}\cdot(\mathbf{a}_2-\mathbf{a}_3)}+e^{i\mathbf{k}\cdot(\mathbf{a}_3-\mathbf{a}_2)}+e^{i\mathbf{k}\cdot(\mathbf{a}_1-\mathbf{a}_3)}+e^{i\mathbf{k}\cdot(\mathbf{a}_3-\mathbf{a}_1)} ,$$

$$g_{27}=(e^{i\mathbf{k}\cdot(\mathbf{a}_2-\mathbf{a}_1)}-e^{i\mathbf{k}\cdot(\mathbf{a}_1-\mathbf{a}_2)})+\tfrac{1}{2}(e^{i\mathbf{k}\cdot(\mathbf{a}_2-\mathbf{a}_3)}-e^{i\mathbf{k}\cdot(\mathbf{a}_3-\mathbf{a}_2)})+\tfrac{1}{2}(e^{i\mathbf{k}\cdot(\mathbf{a}_3-\mathbf{a}_1)}-e^{i\mathbf{k}\cdot(\mathbf{a}_1-\mathbf{a}_3)}) ,$$

$$g_{28}=\tfrac{1}{2}\sqrt{3}(e^{i\mathbf{k}\cdot(\mathbf{a}_3-\mathbf{a}_1)}-e^{i\mathbf{k}\cdot(\mathbf{a}_1-\mathbf{a}_3)})+\tfrac{1}{2}\sqrt{3}(e^{i\mathbf{k}\cdot(\mathbf{a}_3-\mathbf{a}_2)}-e^{i\mathbf{k}\cdot(\mathbf{a}_2-\mathbf{a}_3)}) ,$$

$$g_{29}=\tfrac{1}{4}(e^{i\mathbf{k}\cdot(\mathbf{a}_1-\mathbf{a}_3)}+e^{i\mathbf{k}\cdot(\mathbf{a}_3-\mathbf{a}_1)})+\tfrac{1}{4}(e^{i\mathbf{k}\cdot(\mathbf{a}_2-\mathbf{a}_3)}+e^{i\mathbf{k}\cdot(\mathbf{a}_3-\mathbf{a}_2)})+(e^{i\mathbf{k}\cdot(\mathbf{a}_2-\mathbf{a}_1)}+e^{i\mathbf{k}\cdot(\mathbf{a}_1-\mathbf{a}_2)}) ,$$

$$g_{30}=\tfrac{3}{4}(e^{i\mathbf{k}\cdot(\mathbf{a}_1-\mathbf{a}_3)}+e^{i\mathbf{k}\cdot(\mathbf{a}_3-\mathbf{a}_1)})+\tfrac{3}{4}(e^{i\mathbf{k}\cdot(\mathbf{a}_2-\mathbf{a}_3)}+e^{i\mathbf{k}\cdot(\mathbf{a}_3-\mathbf{a}_2)}) ,$$

$$g_{31}=\tfrac{1}{4}\sqrt{3}(e^{i\mathbf{k}\cdot(\mathbf{a}_3-\mathbf{a}_1)}+e^{i\mathbf{k}\cdot(\mathbf{a}_1-\mathbf{a}_3)}-e^{i\mathbf{k}\cdot(\mathbf{a}_3-\mathbf{a}_2)}-e^{i\mathbf{k}\cdot(\mathbf{a}_2-\mathbf{a}_3)}) .$$

[1] S. C. Shin, J. E. Hilliard, and J. B. Ketterson, J. Vac. Sci. Technol. A **2**, 296 (1984).

[2] A. DiVenere, X. J. Yi, C. L. Hou, H. C. Wang, J. B. Ketterson, G. K. Wong, and I. K. Sou, Appl. Phys. Lett. **62**, 2640 (1993).

[3] T. D. Golding, J. A. Dura, W. C. Wang, A. Vigliante, S. C. Moss, H. C. Chen, J. H. Miller, Jr., C. A. Hoffman, and J. R. Meyer, Appl. Phys. Lett. **63**, 1098 (1993).

[4] J.-P. Issi, Aust. J. Phys. **32**, 585 (1979).

[5] C. A. Hoffman, J. R. Meyer, F. J. Bartoli, A. DiVenere, X. J. Yi, C. L. Hou, H. C. Wang, J. B. Ketterson, and G. K. Wong, Phys. Rev. B **48**, 11 431 (1993).

[6] J. R. Meyer, F. J. Bartoli, E. R. Youngdale, and C. A. Hoffman, J. Appl. Phys. **70**, 4317 (1991).

[7] L. D. Hicks, T. C. Harman, and M. S. Dresselhaus, Appl. Phys. Lett. **63**, 3230 (1993).

[8] T. D. Golding, J. A. Dura, W. C. Wang, J. T. Zborowski, A. Vigliante, H. C. Chen, J. H. Miller, Jr., and J. R. Meyer, Semicond. Sci. Technol. **8**, S117 (1993).

[9] T. D. Golding (private communication).

[10] J. N. Schulman and Yia-Chung Chang, Phys. Rev. B **31**, 2056 (1985).

[11] Yia-Chung Chang, Phys. Rev. B **37**, 8215 (1988).

[12] P. Vogl, H. P. Hjalmarson, and J. D. Dow, J. Phys. Chem. Solids **44**, 365 (1983).

[13] D. J. Chadi, Phys. Rev. B **16**, 790 (1977).

[14] S. Mase, J. Phys. Soc. Jpn. **13**, 434 (1958); **14**, 584 (1959).

[15] J. H. Xu, E. G. Wang, C. S. Ting, and W. P. Su, Phys. Rev. B **48**, 17 271 (1993).

[16] X. Gonze, J.-P. Michenaud, and J.-P. Vigneron, Phys. Rev. B **41**, 11 827 (1990).

[17] L. M. Falicov and P. J. Lin, Phys. Rev. **141**, 562 (1966).

[18] S. Golin, Phys. Rev. **166**, 643 (1968).

[19] J. C. Slater and G. F. Koster, Phys. Rev. **94**, 1498 (1954).

[20] P. O. Löwdin, J. Chem. Phys. **18**, 365 (1950).

[21] G. Bastard, J. A. Brum, and R. Ferreira, Solid State Phys. **44**, 229 (1991).

[22] L. M. Falicov and S. Golin, Phys. Rev. **137**, A871 (1965).

[23] D. Liberman, J. T. Waber, and D. T. Cromer, Phys. Rev. **137**, A27 (1965).

[24] M. P. Vecchi and M. S. Dresselhaus, Phys. Rev. B **10**, 771 (1974).

[25] W. A. Harrison, *Electronic Structure and the Properties of Solids* (Dover, New York, 1989).

[26] D. J. Chadi, in *Atomic Simulation of Materials, Beyond Pair*

Potentials, edited by V. Vitek and D. J. Srolovitz (Plenum, New York, 1989), p. 309.
[27]J. L. Mercer and M. Y. Chou, Phys. Rev. B **49**, 8506 (1994).
[28]J. Rose and R. Schuchardt, Phys. Status Solidi B **117**, 213 (1983).
[29]L. Ley, R. A. Pollak, S. P. Kowalczyk, R. McFeely, and D. A. Shirley, Phys. Rev. B **8**, 641 (1973).
[30]P. Y. Wang and A. L. Jain, Phys. Rev. B **2**, 2978 (1970).
[31]O. Hunderi, J. Phys. F **5**, 2214 (1975).
[32]H. R. Verdún and H. D. Drew, Phys. Rev. B **14**, 1370 (1976).
[33]R. T. Isaacson and G. A. Williams, Phys. Rev. **185**, 682 (1969).
[34]R. T. Bate, N. G. Einspruch, and P. J. May, Jr., Phys. Rev. **186**, 599 (1969).
[35]J. P. Omaggio, J. R. Meyer, C. A. Hoffman, A. DiVenere, X. J. Yi, C. L. Hou, H. C. Wang, J. B. Ketterson, G. K. Wong, and J. P. Heremans, Phys. Rev. B **48**, 11 439 (1993).
[36]V. de Renzi, M. G. Betti, and C. Mariani, Surf. Sci. **287/288**, 550 (1993).
[37]R. N. Brown, J. G. Mavroides, and B. Lax, Phys. Rev. **129**, 2055 (1963).
[38]M. Maltz and M. S. Dresselhaus, Phys. Rev. B **2**, 2877 (1970).
[39]P. W. Chao, H. T. Chu, and Y. H. Kao, Phys. Rev. B **9**, 4030 (1974).
[40]G. E. Smith, G. A. Baraff, and J. M. Rowell, Phys. Rev. **135**, A1118 (1964).
[41]V. S. Edel'man, Adv. Phys. **25**, 555 (1976).
[42]S. Takaoka, H. Kawamura, K. Murase, and S. Takano, Phys. Rev. B **13**, 1428 (1976).
[43]R. T. Isaacson and G. A. Williams, Phys. Rev. **177**, 738 (1969).
[44]M. S. Dresselhaus and J. G. Mavroides, Phys. Rev. Lett. **14**, 259 (1965).
[45]M. S. Dresselhaus and J. G. Mavroides, *Optical Properties and Electronic Structure of Metals and Alloys,* edited by F. Abelès (North-Holland, Amsterdam, 1966), p. 508.
[46]S. Takano, M. Koga, and Y. Matsumoto, J. Phys. Soc. Jpn. **44**, 453 (1978).
[47]W. R. Datars and J. Vanderkooy, IBM J. Res. Dev. **8**, 247 (1964).
[48]L. R. Windmiller, Phys. Rev. **149**, 472 (1966).
[49]R. A. Herrod, C. A. Gage, and R. G. Goodrich, Phys. Rev. B **4**, 1033 (1971).
[50]J. Ketterson and Y. Eckstein, Phys. Rev. **132**, 1885 (1963).
[51]S. J. Freeman and H. J. Juretschke, Phys. Rev. **124**, 1379 (1961).